Hindawi
Mathematical Problems in Engineering
Volume 2020, Article ID 3268694, 15 pages
https://doi.org/10.1155/2020/3268694

Research Article

A Novel Intelligent Method for Predicting the Penetration Rate of the Tunnel Boring Machine in Rocks

Yan Zhang,[1,2] Mingdong Wei ,[3] Guoshao Su,[2] Yao Li,[4] Jianbin Zeng,[1] and Xueqin Deng[1]

[1]*Guangxi Key Laboratory of New Energy and Building Energy Saving, College of Civil and Architecture Engineering, Guilin University of Technology, Guilin 541004, China*
[2]*Guangxi Key Laboratory of Disaster Prevention and Engineering Safety, College of Civil Engineering and Architecture, Guangxi University, Nanning 530004, China*
[3]*State Key Laboratory of Hydraulics and Mountain River Engineering, College of Water Resource and Hydropower, Sichuan University, Chengdu 610065, China*
[4]*Water Authority of Zizhong County, Neijiang 641200, Sichuan, China*

Correspondence should be addressed to Mingdong Wei; weimingdong@163.com

Received 11 May 2020; Revised 16 July 2020; Accepted 17 August 2020; Published 4 September 2020

Academic Editor: Nhon Nguyen-Thanh

In the construction of rock tunnels, the penetration rate of the tunnel boring machine (TBM) is influenced by many factors (e.g., geomechanical parameters), some of which are highly uncertain. It is difficult to establish a precise model for predicting the penetration rate on the basis of the influencing factors. Thus, this work proposed a useful method, based on the relevance vector machine (RVM) and particle swarm optimization (PSO), for the prediction of the TBM penetration rate. In this method, the RVM played a vital role in establishing a nonlinear mapping relationship between the penetration rate and its influencing factors through training-related samples. Then, the penetration rate could be predicted using some collected data of the influencing factors. As for the PSO, it helped to find the optimum value of a key parameter (called the basis function width) that was needed in the RVM model. Subsequently, the validity of the proposed RVM-PSO method was checked with the data monitored from a rock tunnel. The results showed that the RVM-PSO method could estimate the penetration rate of the TBM, and it proved superior to the back-propagation artificial neural network, the least-squares support vector machine, and the conventional RVM methods, in terms of the prediction performance. Moreover, the proposed RVM-PSO method could be applied to identify the difference in the importance of the various factors affecting the TBM penetration rate prediction for a tunnel.

1. Introduction

As a consequence of sustained interest in the development of underground space, tunnels play a more and more important role in human production activities and life. For example, there are many tunnels under construction in hydraulic engineering (e.g., transportation tunnels, drainage tunnels, and grouting tunnels [1–3]) and in traffic engineering (road tunnels). Thus, considerable scientific efforts have been made to develop advanced methods, techniques, and theories for improving the safety and efficiency of tunnel constructions [4–11]. In the recent decades, the tunnel boring machine (TBM) has been widely applied to tunnel constructions, in general, and long tunnels in particular, due to its many superior performances over the traditional new Austrian tunnelling method (NATM) and drilling-blasting methods, such as less pollution to the surrounding environment and higher safety, efficiency, and quality. The penetration rate of the TBM affects not only the construction schedule and the amount of capital cost but also the stability of surrounding rock mass during tunnelling. Hence, it is significant to accurately predict the penetration rate for improving construction efficiencies and reducing construction risks.

Researchers have never ceased to develop empirical and theoretical models for evaluating the penetration rate/performance of the TBM since it was invented. Some typical models are the Q_{TBM} model [12], the Field Penetration Index (FPI) model [13], the Specific Rock Mass Boreability Index (SRMBI)

model [14], the Colorado School of Mines (CSM) model [15], and the Norwegian University of Science and Technology (NTNU) model [16]. Among them, the CSM and NTNU are the most famous models and are widely used. The CSM model is established on the basis of laboratory test results and by analyzing the rock-breaking mechanism of the TBM. This model has the advantage that it can take into account the influence of the strength and brittleness of rock on the penetration rate. However, the original CSM model has not considered the effect of joint cracks in rock masses, which can significantly affect the TBM performance. For this reason, much research attention has been paid to replacing the compressive strength of rock with that of the rock mass, in order to consider the effect of joint cracks. Even still, the modified CSM mode, however, cannot meet the accuracy requirement for many complicated rock structures. In addition, there are only a few engineering factors considered in the derivation process of the CSM model, restricting the ability of the model to solve complex engineering problems. The NTNU model not only considers the properties of the TBM but also involves the interaction between hobs and rock mass. Moreover, all empirical parameters involved in this model are obtained from practical tunnel engineering by using back analysis; thus, the NTNU model has received a certain degree of engineering application. Nevertheless, the experiments to determine the rock drillability and the friction coefficient between rock mass and hobs are not commonly conducted in the rock mechanics community; the acquisition of these parameters limits the application of the model somewhat.

In the recent years, with the rapid development of artificial intelligence (AI) technology, many intelligent models, such as the artificial neural network (ANN) [17, 18], support vector machine (SVM) [19, 20], group method of data handling (GMDH) [21], and adaptive neurofuzzy inference system (ANFIS) [22], have been applied to predicting the penetration rate. For example, there are a number of intelligent prediction models based on the dataset from the Queens Water Tunnel #3 (New York City, USA) (see Table 1), which is also used in this study to assess the proposed method. These models have a typical advantage that they can establish the complicated nonlinear relationship between the penetration rate and various influencing factors with no need to consider too many indeterminate mechanical mechanisms, which simplifies the problem of estimating the penetration rate. However, they also have some deficiencies. For example, it is difficult for the ANN to determine an appropriate network topology and reasonable hyperparameter values. As for the SVM, its parameters are always obtained by manual trials, which often contain a certain degree of subjectivity and blindness. To circumvent these issues, many researchers prefer using the optimization methods/algorithms, i.e., particle swarm optimization (PSO), cuckoo search (CS), and genetic programming (GP), to search the optimal hyperparameters for the prediction models [33]. Then, some hybrid models have been developed by combining the optimization methods with the intelligent models, including the PSO-ANN [34], PSO-SVM [35], and GP-ANN [36]. Although these hybrid models can solve the problem of parameter determination, they still have limitations, such as relatively low accuracy of ANN-based models and comparatively high computational cost/time of SVM-based models. Until now, a well-recognized model that can overcome all the problems mentioned above has not emerged. For the penetration rate prediction, it is, thus, necessary to explore a high-efficiency and accurate-enough model that can not only solve the parameter determination problem but also obtain better prediction results.

To address this issue, a useful method is developed in this study for predicting the TBM penetration rate by integrating the PSO optimization algorithm into the relevance vector machine (RVM) method. In the proposed method, the RVM contributes to establishing a nonlinear mapping relationship between the penetration rate and its various influencing factors, and PSO helps to optimize the parameter of the RVM. There is only one parameter (i.e., the basis function width) needed to determine during the use of the RVM, for which fewer parameters are required than the ANN and SVM. Compared with the ANN, the RVM has a higher prediction precision, and moreover, it utilizes fewer basis functions and requires lower computational cost than the SVM. Besides, the RVM has many additional advantages, such as a small number of samples required and non-"Mercer" kernels [37]. Moreover, PSO is an excellent stochastic search optimization method with the characteristics of simple computation and rapid convergence capability, and it is widely applied to various complicated optimization problems [38]. Thus, the RVM-PSO method makes full use of the merits of both PSO and the RVM and possesses a better prediction performance for the TBM penetration rate.

2. Methodology

The two main parts (i.e., RVM and PSO) of the RVM-PSO method developed in this study will be introduced herein.

2.1. The RVM Model. The RVM model is firstly proposed by Tipping [39] on the basis of the Sparse Bayesian Learning theory, which is a probabilistic model to remedy the defects of the SVM. The principle of the RVM is as follows.

It is well known that many problems involving machine learning would meet the supervised learning, in which a set of learning examples (number: N) is given as $\{x_n, t_n\}_{n=1}^{N}$, where $\boldsymbol{x}_n$ denotes an input vector and t_n represents a scalar output or target. Then, the relationship between $\boldsymbol{x}_n$ and t_n is described as

$$t_n = y(\mathbf{x}_n, \boldsymbol{\omega}) + \xi_n, \tag{1}$$

where $y(\mathbf{x}_n, \omega)$ is expressed as equation (2), and it has a linear relationship with basis functions $\phi(\mathbf{x}_n)$. $\boldsymbol{\omega}$ is the weight matrix. ξ_n is the Gaussian noise obeying the normal distribution with a mean of 0 and a variance of σ^2. Hence, the expression $p(t_n \mid \mathbf{x}) = N(t_n \mid y(\mathbf{x_n}), \sigma^2)$ belongs to a Gaussian distribution determined by t_n, $y(\mathbf{x_n})$ and σ^2.

$$y(\mathbf{x}_n, \boldsymbol{\omega}) = \sum_{n=1}^{N} \omega_n \phi(\mathbf{x}_n) = \boldsymbol{\omega}^T \boldsymbol{\varphi}, \tag{2}$$

Table 1: Review of several TBM performance prediction models using the dataset from the Queens Water Tunnel #3.

Reference	Model	Main factors	Predicted value	Evaluation parameter
Yagiz [13]	SA	UCS, BTS, BI, DPW, α, FN	FPI	R^2, r
Gholamnejad and Tayarani [18]	ANN	DPW, UCS, RQD	PR	MSE, R^2
Mahdevari et al. [19]	SVM	UCS, BTS, BI, DPW, α, SE, TF, CP, CT	PR	MSE, R^2
Yagiz et al. [23]	ANN	DPW, UCS, BI, α	PR	RMSE, VAF, r
Mikaeil et al. [24]	FIS	DPW, UCS, BTS, α, PSI	PR	DPDO
Wen et al. [25]	BP-ANN	UCS, BTS, SWP, PSI, α	PR	MRE
Yagiz and Karahan [26]	PSO	UCS, BTS, BI, DPW, α	PR	MSE
Ghasemi et al. [27]	FIS	UCS, BI, DPW, α	PR	VAF, RMSE
Yagiz and Karahan [28]	DE, HS-BFGS, GWO	DPW, UCS, BI, α	PR	MSE
Mikaeil et al. [29]	EMFE	UCS, PSI, DPW, α	PR	R^2
Naghadehi et al. [30]	GEP	UCS, BTS, BI, DPW, α	PR, FPI	R^2, RMSE, MAPE
Naghadehi et al. [31]	ICA, CART, GEP	UCS, BTS, DPW, BI, α	PR	R^2, RMSE, MAPE
Naghadehi et al. [32]	GEP, ICA	UCS, BTS, DPW, BI, α	PR	R^2, RMSE, MAPE

Nomenclature in this table: brittleness index (BI); Brazilian tensile strength (BTS); classification and regression tree (CART); cutterhead power (CP); cutterhead torque (CT); differential evolution (DE); Dubois–Prade decision operator (DPDO); distance between planes of weakness (DPW); extended multifactorial fuzzy evaluation (EMFE); field penetration index (FPI); gene expression programming (GEP); grey wolf optimizer (GWO); hybrid harmony search (HS-BFGS); imperialist competitive algorithm (ICA); individual cutter force (FN); mean absolute percentage error (MAPE); mean relative error (MRE); mean squared error (MSE); penetration rate (PR); peak slope index (PSI); coefficient of correlation (R^2); root mean square error (RMSE); rock quality designation (RQD); coefficient of the cross correlation (r); statistical analysis (SA); specific energy (SE); the spacing between the weakness planes (SWP); thrust force (TF); uniaxial compressive strength of intact rock (UCS); variance accounted for (VAF); angle between the longitudinal tunnel axis and the plane of weakness (α).

where $\phi(\mathbf{x}_n)$ is often identified with the Gaussian radial basis function parameterized by training vectors, as shown in the following equation:

$$\phi(\mathbf{x}_n) = \exp\left(-\frac{\|\mathbf{x}-\mathbf{x}_n\|^2}{2r^2}\right), \tag{3}$$

where r is the width of radial basis function, which is an important parameter affecting the accuracy of prediction results. With the assumption of independence to t_n, the complete probability expression for the sample dataset can be written as

$$p\left(\mathbf{t}\,|\,\boldsymbol{\omega},\sigma^2\right) = \left(2\pi\sigma^2\right)^{-(N/2)}\exp\left\{-\frac{1}{2\sigma^2}\|\mathbf{t}-\boldsymbol{\Phi}\boldsymbol{\omega}\|^2\right\}, \tag{4}$$

where $t = (t_1\, t_2, \ldots, t_N)^T$ and $\omega = (\omega_0\, \omega_1, \ldots, \omega_N)^T$. $\Phi = [\phi(\mathbf{x}_1)\,\phi(\mathbf{x}_2), \ldots, \phi(\mathbf{x}_N)]^T$ is a $N \times (N+1)$ design matrix. The maximum-likelihood estimations of $\boldsymbol{\omega}$ and σ^2 can lead to overfitting for training because many parameters of learning samples are used. Thus, some additional constraints are generally exerted to solve this problem. The Bayesian perspective is usually adopted for the RVM to constrain the parameters by defining a simpler function of $\boldsymbol{\omega}$, which is shown as follows:

$$p(\boldsymbol{\omega}\,|\,\boldsymbol{\alpha}) = \prod_{i=0}^{N} N\left(\boldsymbol{\omega}_i\,|\,0,\alpha_i^{-1}\right), \tag{5}$$

where α is a vector with $N+1$ hyperparameters. Then, there are individual distributed parameters for every weight. Thus, the complexity of the prior distribution can be greatly reduced. In order to match the final function, a noise variance σ^2 is added for α. These quantities belong to the scale parameters, for which the priors are the Gamma distribution:

$$p(\boldsymbol{\alpha}) = \prod_{i=0}^{N} \text{Gamma}\,(\alpha_i\,|\,a,b),$$

$$p(\beta) = \text{Gamma}\,(\beta\,|\,c,d), \tag{6}$$

where $\beta = \sigma^2$ and

$$\text{Gamma}\,(\alpha\,|\,a,b) = \Gamma(a)^{-1}b^a\alpha^{a-1}e^{-b\alpha}. \tag{7}$$

In equation (7), $\Gamma(a) = \int_0^\infty t^{a-1}e^{-t}\mathrm{d}t$ is the Gamma function. To ensure that these parameters have no prior information, it is better to set them to small values. If they are fixed to $a = b = c = d = 0$, more uniform hyperparameters can be obtained, and therefore, most of the related literature adopt this parameter setting strategy. To help to understand the general idea of this introduction, a visual implementation process is shown in Figure 1.

On the basis of the prior, the probabilistic distribution of the posterior is given as equation (8) by following Bayes' rule.

$$p\left(\boldsymbol{\omega},\boldsymbol{\alpha},\sigma^2\,|\,\mathbf{t}\right) = \frac{P\left(\mathbf{t}\,|\,\boldsymbol{\omega},\boldsymbol{\alpha},\sigma^2\right)P\left(\boldsymbol{\omega},\boldsymbol{\alpha},\sigma^2\right)}{p(\mathbf{t})}. \tag{8}$$

By assuming that there is a new prediction sample $(\mathbf{x}*, *)$, the predictive distribution can be written as

$$p(t^*\,|\,\mathbf{t}) = \int p\left(t^*\,|\,\boldsymbol{\omega},\boldsymbol{\alpha},\sigma^2\right)p\left(\boldsymbol{\omega},\boldsymbol{\alpha},\sigma^2\,|\,\mathbf{t}\right)\mathrm{d}\omega\mathrm{d}\alpha\mathrm{d}\sigma^2, \tag{9}$$

where $p(\omega,\alpha,\sigma^2\,|\,\mathbf{t})$ cannot be directly computed, so it is decomposed as follows:

$$p\left(\boldsymbol{\omega},\boldsymbol{\alpha},\sigma^2\,|\,\mathbf{t}\right) = p\left(\boldsymbol{\omega}\,|\,\mathbf{t},\boldsymbol{\alpha},\sigma^2\right)p\left(\boldsymbol{\alpha},\sigma^2\,|\,\mathbf{t}\right). \tag{10}$$

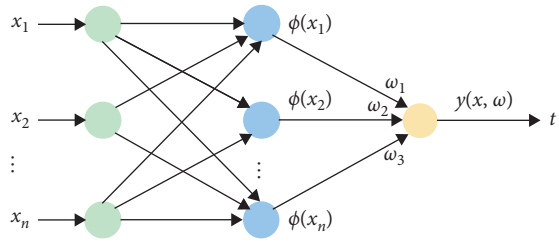

FIGURE 1: A schematic of the implementation process of the RVM.

Based on the abovementioned introduction, the posterior distribution of $\boldsymbol{\omega}$ is given by

$$p\left(\boldsymbol{\omega} \mid \mathbf{t}, \boldsymbol{\alpha}, \sigma^2\right) = \frac{p\left(\mathbf{t} \mid \boldsymbol{\omega}, \sigma^2\right) p\left(\boldsymbol{\omega} \mid \boldsymbol{\alpha}\right)}{p\left(\mathbf{t} \mid \boldsymbol{\alpha}, \sigma^2\right)} = N\left(\boldsymbol{\mu}, \sum\right), \tag{11}$$

where the posterior mean μ and covariance $\sum$ are given in equations (12) and (13), respectively:

$$\boldsymbol{\mu} = \sigma^{-2} \sum \boldsymbol{\Phi}^T \mathbf{t}. \tag{12}$$

$$\sum = \left(\sigma^{-2} \boldsymbol{\Phi}^T \boldsymbol{\Phi} + \mathbf{A}\right)^{-1}, \tag{13}$$

where $\mathbf{A}$ is the diagonal matrix $\mathbf{A} = \text{diag}\,(\alpha_0, \alpha_1, \ldots, \alpha_N)$.

When the hyperparameters are updated to learn, many of ω_i $(i = 1, 2, \ldots, N)$ tend to be zero, so that only a few basis functions (relevance vectors) can work on the results. Thus, the goal of sparseness is achieved.

By training the learning samples $\{\mathbf{x}_n, t_n\}_{n=1}^N$, the prediction could proceed on the basis of the posterior distribution over the weights. After maximizing the hyperparameters, the optimal parameters α_{MP} and σ^2_{MP} can be found. The predictive distribution can be computed by equation (9). For a new prediction sample $(\mathbf{x}^*, *)$, the predictive probability is given by

$$p\left(t^* \mid \mathbf{t}, \boldsymbol{\alpha}_{\text{MP}}, \sigma^2_{\text{MP}}\right) = \int p\left(t^* \mid \boldsymbol{\omega}, \sigma^2_{\text{MP}}\right) p\left(\boldsymbol{\omega} \mid \mathbf{t}, \boldsymbol{\alpha}_{\text{MP}}, \sigma^2_{\text{MP}}\right) \mathrm{d}\boldsymbol{\omega}. \tag{14}$$

Both of the two integrands on the right-hand side of equation (14) are Gaussian distributions, so $*$ also belongs to a Gaussian distribution, which is computed by

$$p\left(t^* \mid \mathbf{t}, \boldsymbol{\alpha}_{\text{MP}}, \sigma^2_{\text{MP}}\right) = N\left(t^* \mid y^*, \sigma^2_*\right). \tag{15}$$

Then, the mean y^* and the covariance σ^2_* are, respectively, given as

$$\begin{aligned} y^* &= \boldsymbol{\mu}^T \phi\left(\mathbf{x} *\right), \\ \sigma^2_* &= \sigma^2_{\text{MP}} + \phi\left(\mathbf{x}^*\right)^T \sum \phi\left(\mathbf{x}^*\right). \end{aligned} \tag{16}$$

2.2. The PSO Algorithm. Particle swarm optimization is an evolutionary computation technology based on the swarm intelligence method, which was proposed by Kennedy and Eberhart [40] and first intended for simulating social behavior. PSO is similar to the genetic algorithm (GA); both of them are optimization tools based on population information. However, unlike GA, PSO does not need crossover and mutation, and it finds the best solution by tracking the optimum particles. Compared with GA, PSO has the merits of a simpler implementation process and a better intelligent background, and it is not only used in scientific research but also applied to engineering practices in the industry [41].

To solve the optimization problem, PSO is initialized with a generation of random particles first (the number of particles is denoted as NP) and, then, searches for the optimum by updating generations. In PSO, the potential solutions, i.e., particles, fly through the problem space by following the current optimum particles. Each particle keeps track of its coordinates (in the problem space), which are associated with the best solution that the current-generation particles have achieved so far. This value is called *p*best. Another "best" value tracked by the particle swarm optimizer is the best value obtained so far by all particles; this value is a global best called *gbest*. After finding the two best values, the particles update their velocities and positions according to the following equation:

$$\left.\begin{aligned} v_{id} &= w v_{id} + c_1 r_1 \left(p_{id} - x_{id}\right) + c_2 r_2 \left(p_{gd} - x_{id}\right) \\ x_{id} &= x_{id} + v_{id} \end{aligned}\right\}, \tag{17}$$

where v_{id} is the velocity vector. x_{id} is the position vector. p_{id} represents the best position in the current stage of particle I, and the corresponding fitness is *p*best. p_{gd} denotes the global best position in the process of particle iteration on the dth dimension, and its fitness is *g*best. The parameters r_1 and r_2 are two random values uniformly distributed in [0, 1] [42]. c_1 and c_2 are acceleration constants, which can guide the particle on how to follow the *p*best and the *g*best. Small values of c_1 and c_2 may cause the particle to vibrate out of the target region; conversely, the large values can make the particle fly rapidly towards the target region and even surpass the target region. c_1 and c_2 usually have the same value between 1.8 and 2.0. The parameter w represents the inertia weight, which controls the influence of the previous velocity on the new velocity. When w is large, the algorithm has a strong ability of global search, while a small w value can make the algorithm have a strong ability of local search. The inertia weight w can be determined by the following equation:

$$w = w_{\max} - \frac{w_{\max} - w_{\min}}{t_{\max}} t, \tag{18}$$

where t is the current iteration step, $t_{\max}$ is the maximum iteration step, $w_{\max}$ is the maximum inertia weight, and $w_{\min}$ is the minimum inertia weight. In general, $w_{\max} = 0.9$ and $w_{\min} = 0.4$ [43].

A schematic diagram is given in Figure 2 to show how PSO solves the global optimization problem. In Figure 2, a two-dimensional problem is assumed. The red point represents $p_{gd.}$ The velocity of particle i is updated by three parts, denoted as v_1, v_2, and v_3. $v_1 = c_1 r_1 \left(p_{id} - x_{id}\right)$ is the velocity of particle i caused by p_{id}; $v_2 = w v_{id}$ is the velocity resulted from the initial velocity; and $v_3 = c_2 r_2 \left(p_{gd} - x_{id}\right)$ is the velocity induced by $p_{gd.}$ Then, the particle i is updated to a new position. By following the same way, the location of

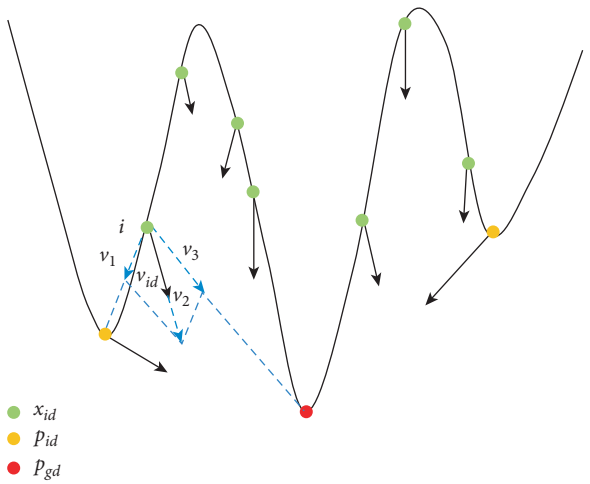

Figure 2: A schematic of PSO for solving the global optimization problem.

particle i continues to be updated and gradually approaches the global optimal solution.

2.3. The RVM-PSO Method. Since the RVM contributes to establishing a nonlinear mapping relationship between the output/target and input vectors and PSO helps significantly to optimize the parameter (i.e., the basis function width) of the RVM, the RVM-PSO method is developed by integrating PSO into the RVM. The implementation steps of the RVM-PSO method are as follows.

First, one should analyze and process the collected data to get the input and output datasets for the RVM-PSO model. For example, the output parameter is the penetration rate in this study, and the input parameters are the influencing factors. Given that the input parameters are usually not in the same order of magnitude and this fact will affect the learning result, the data should be normalized. The principles for normalization are expressed as

$$a_i = \frac{x_i}{s}, \qquad b_i = y_i - \overline{y}, \tag{19}$$

where a_i and b_i are the normalized values, x_i denotes an i-dimensional input vector, y_i represents the output of the ith sample, $\overline{y}$ is the mean of all y_i values, and s is determined using the following equation:

$$s = \left(\frac{1}{n-1} \sum_{i=1}^{n} \left(x_i - \overline{x} \right)^2 \right)^{(1/2)}, \qquad x = \frac{1}{n} \sum_{i=1}^{n} x_i,\ y = \frac{1}{n} \sum_{i=1}^{n} y_i. \tag{20}$$

Subsequently, the normalized values of input and output data are employed to establish training sets, which can be used for training and fitting to find the nonlinear relation between the input and output data.

In the next step, PSO program should be started to generate the particles, which are treated as the widths of the basis function to be involved in the RVM model. The RVM model should be optimized automatically by updating the particles in PSO to reduce the error between the predicted results and the expected results until the prediction corresponding to a certain hyperparameter meets the accuracy requirement. A flow chart of the detailed implementation process of the RVM-PSO method is shown in Figure 3.

3. Application of the Prediction Methods to an Engineering Practice

To check the validity of the developed RVM-PSO method on the TBM penetration rate prediction, the method will be applied to estimate the penetration rate data collected from the Queens Water Tunnel #3 (New York City, USA) [25, 44], and then, the predicted values will be compared with the actual values. Moreover, the prediction performance of the RVM-PSO method will be compared with that of the back-propagation artificial neural network (BP-ANN) [25], the least-squares support vector machines (LS-SVM), and the conventional RVM methods, which have already been widely applied to nonparametric and nonlinear classification and forecasting problems. For assessing our proposed RVM-PSO method by comparing the results with those from the BP-ANN method, this study adopted the same data as those used in the BP-ANN method in reference [25], that is, the data in Table 2.

3.1. Implementation of the RVM-PSO Method. Note that the factors affecting the TBM penetration rate are too many to consider all of them in a prediction model. For this reason, it is, thus, common to consider only the relatively significant influencing factors in the applications of the current intelligent prediction methods. In addition, since the TBM machines used during the whole tunnelling process of the Queens Water Tunnel #3 are identical, some mechanical and geometrical parameters of TMB machines, such as the hob radius, the thickness of the hob end, and the rated thrust of a single hob, are not the main factors to induce the variation of penetration rate data recorded in that tunnelling practice. Hence, these parameters are not considered in this case study. Five parameters are tentatively speculated as to the main factors affecting the TBM penetration rate of the Queens Water Tunnel #3, and they are involved in the penetration rate prediction model established here. The five main factors are the angle between the longitudinal tunnel axis and the plane of weakness (α), the uniaxial compressive strength of intact rock (UCS), the Brazilian tensile strength (BTS), the spacing between the weakness planes (SWP) [45, 46], and the peak slope index (PSI, i.e., the ratio of the maximum force to the corresponding displacement in the impact test [47–54]).

Table 2 lists the penetration rate data corresponding to different values of the main influencing factors. Fifteen groups of the data are randomly selected as learning samples (denoted

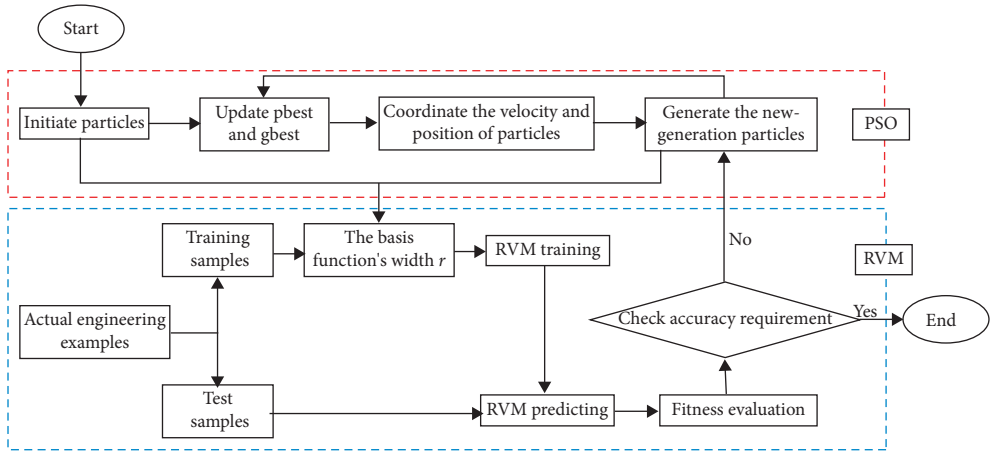

Figure 3: A flow chart of the RVM-PSO method used for predicting a target variable.

Table 2: Dataset of the TBM penetration rate (PR) collected from the Queens Water Tunnel #3.

Sample no.	α (°)	UCS (MPa)	BTS (MPa)	SPW (m)	PSI (kN/mm)	PR (m/h)
L1	52	141.4	9.4	1.6	26	1.74
L2	28	153.4	9.1	2	23	1.94
L3	44	147.6	10.8	2	30	2.09
L4	11	131	9.9	0.4	32	1.78
L5	28	140.7	9.1	1.6	38	2.1
L6	33	173.1	9.8	0.8	31	1.84
L7	71	176	10.3	2	30	1.6
L8	81	150.7	10.8	1.6	30	1.98
L9	83	125	8.3	1.6	27	2.21
L10	69	129.2	8.2	0.8	29	1.84
L11	73	134.5	9	0.2	26	2.01
L12	55	192.7	11.4	0.4	42	2.18
L13	66	182.4	10.2	0.8	39	2
L14	74	159	8.7	0.2	36	2.28
L15	51	156.9	10.7	0.8	30	2.16
T1	40	189	9	2	56	2.2*
T2	34	191	10.4	0.4	54	2.95*
T3	70	137.2	8.8	1.6	42	2.2*
T4	32	136.2	9.2	0.4	40	2.03*
T5	10	128.6	9.9	1.6	32	1.75*
T6	11	131	9.9	0.4	32	1.78*
T7	50	138.6	10	0.2	30	2.39*
T8	18	133.4	10.5	1.6	30	1.6*
T9	52	154.5	10.1	2	33	1.58*
T10	33	173.1	9.8	0.8	31	1.84*

as L1 to L15), and the remaining ten groups are assigned as test samples (represented as T1 to T10). In the RVM-PSO model established here, the penetration rate and the main influencing factors are the output and input parameters, respectively. PSO is employed for the optimization of the Gaussian kernel width. The termination condition is set to $f < 0.03$ (where f is the mean relative error), and the maximum number of iterations is specified as 1000. Parameter settings in PSO are $d = 1$, $NP = 10$, $c_1 = c_2 = 2$, and $V_{\max} = 1$. After establishing the nonlinear relationship between the penetration rate and the influencing factors by training the learning samples, the prediction can be made by inputting some values of the key influencing factors that are measured from the tunnel. In this study, PSO finds the best value of the Gaussian kernel width through the search of three-generation particles. The detailed search process of the particles is shown in Figure 4, which indicates that the particles of a newer generation are closer to the termination condition, and the mean relative error corresponding to one of the third-generation particles is only 0.028, achieving the required accuracy.

3.2. Brief Introduction of the BP-ANN and the LS-SVM Methods. Since the prediction made by the RVM-PSO method will be compared with those by the BP-ANN and the LS-SVM methods, the latter two methods are briefly introduced here.

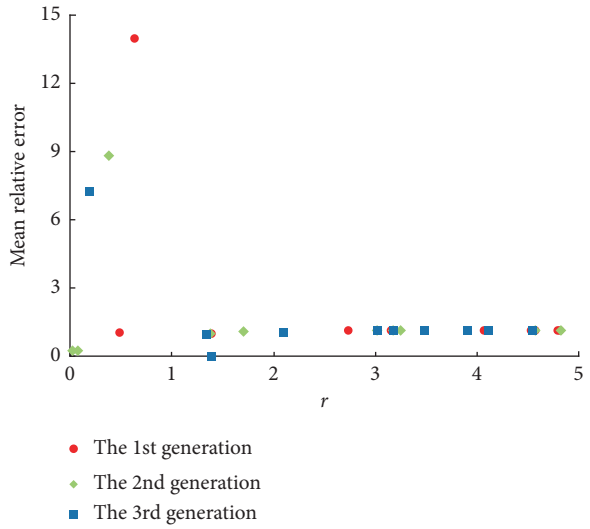

FIGURE 4: The detailed search process of the particles in the RVM-PSO model established for predicting the TBM penetration rate in the Queens Water Tunnel #3.

3.2.1. The BP-ANN Method. The artificial neural network (ANN) is an information system proposed by abstracting, simplifying, and simulating the structure, function, and basic characteristics of the human brain neural network. The back-propagation artificial neural network (BP-ANN), originally developed by McClelland and Rumelhart [55], is a multilayer forward neural network based on the error back-propagation algorithm. As a typical learning algorithm of the ANN, the main structure of the BP-ANN is composed of an input layer, one or more hidden layers, and an output layer. Each layer is composed of a number of neurons (nodes), and the output value of each node is determined by input values, action functions, and thresholds. The BP learning algorithm is used to train multilayer networks and implement a gradient search to minimize the squared error between realized and desired outputs.

The learning process of the network includes two processes: forward information propagation and backward error propagation. In the forward propagation process, the input information is transmitted from the input layer to the output layer through the hidden layer. After the action functions are operated, the output value is compared with the expected value. If there is an error, the error propagates back and returns along the original connection path. By modifying the weight of neurons layer by layer, the error can be reduced, and the loop proceeds until the output result meets the specified accuracy requirement.

The output O_j of neuron j on the hidden or output layer of the BP neural network is determined by the following equation:

$$O_j = f_j\left(\sum \omega_j x_i + \theta\right), \tag{21}$$

where f_j is the excitation function corresponding to neuron j, θ is the threshold of neuron j, x_i denotes the inputs to neuron j, and ω_j represents the connection weight corresponding to the input and neuron j.

3.2.2. The LS-SVM Method. In the least-squares support vector machine method proposed by SuyKens et al. [56], the least-squares linear system is used as the loss function, and the solution process is transformed into solving a set of equations, which dramatically speeds up the solution procedure. Thus, the LS-SVM has achieved good results on pattern recognition and nonlinear estimation. In the use of the LS-SVM, the samples of training data can be expressed as $(X_1, Y_1), (X_2, Y_2), \ldots, (X_l, Y_l)$, where y_i is the target value and $\boldsymbol{x_i}$ is the input vector. The function estimation problem can be described as solving the following question:

$$\min_{\omega,b,e} J(\omega, e) = \frac{1}{2}\omega^T\omega + \gamma\frac{1}{2}\sum_{i=1}^{l} e_i^2. \tag{22}$$

The constraint condition is as follows:

$$y_i = \Phi(x_i) \times w + b + \xi_i, \quad i = 1, 2, \ldots, l, \tag{23}$$

where $\Phi()$: $R^n \longrightarrow R^{nh}$ is the kernel function, ω ($\in R^{nh}$) is the weight vector, ξ_i ($\in R$) is the error variable, b is the deviation value, and γ an adjustable parameter.

The kernel function can map the samples in the original space to a vector in a high-dimensional feature space to solve the linear indivisibility problem, and thus, the optimization problem can be solved using the Lagrangian method:

$$L(\omega, b, e, \alpha) = J(\omega, e) - \sum_{i=1}^{l} \alpha_i\left(\omega^T\Phi(x_k) + b + e_i - y_i\right), \tag{24}$$

where αi ($i = 1, 2, \ldots, l$) is the Lagrange multiplier. The optimization conditions are as follows:

$$\begin{aligned}
&\frac{\partial L}{\partial \omega} = 0 \longrightarrow \omega = \sum_{i=1}^{l} \alpha_i \Phi(x_i),\\
&\frac{\partial L}{\partial b} = 0 \longrightarrow \sum_{i=1}^{l} \alpha_i = 0,\\
&\frac{\partial L}{\partial e_i} = 0 \longrightarrow \alpha_i = \gamma e_i,\\
&\frac{\partial L}{\partial \alpha_i} = 0 \longrightarrow \omega^T\Phi(x_i) + b + e_i - y_i = 0.
\end{aligned} \tag{25}$$

Subsequently, using these optimization conditions, one can get

$$\begin{bmatrix} 0 & 1_v^T \\ -1_v & \Omega + \dfrac{1}{\gamma} I \end{bmatrix} \begin{bmatrix} b \\ \alpha \end{bmatrix} = \begin{bmatrix} 0 \\ y \end{bmatrix}, \tag{26}$$

where $x = [x_1, x_2, \ldots, x_l]$, $y = [y_1, y_2, \ldots, y_l]$, and $\alpha = [\alpha_1, \alpha_2, \ldots, \alpha_l]$. The kernel function K (xk,xl) $(=\Phi(xk)T\Phi(xl))$ is a symmetric function satisfying Mercer's condition.

The regression estimate of the least-squares support vector machine is as follows:

Table 3: Comparison of the predicted results with different methods.

Sample no.	In situ measurement (m/h)	BP-ANN [25]		LS-SVM		RVM		RVM-PSO	
		The predicted results (m/h)	The relative errors (%)	The predicted results (m/h)	The relative errors (%)	The predicted results (m/h)	The relative errors (%)	The predicted results (m/h)	The relative errors (%)
T1	2.2*	2.46	11.82	2.22	0.98	2.18	−0.8	2.18	−0.73
T2	2.95*	3.13	6.1	2.78	−5.72	2.84	−3.73	2.93	−0.68
T3	2.2*	2.19	−0.45	2.1	−4.66	2.06	−6.22	2.13	−3.05
T4	2.03*	2.38	17.24	2.06	1.53	2.04	0.55	2.1	3.48
T5	1.75*	1.74	−0.57	1.78	1.48	1.71	−2.46	1.77	1.37
T6	1.78*	1.61	−9.55	1.89	6.37	1.91	7.25	1.78	0.16
T7	2.39*	2.27	−5.02	2.04	−14.7	2.05	−14.27	2.36	−1.31
T8	1.6*	1.71	6.87	1.80	12.65	1.76	10.18	1.65	3.13
T9	1.58*	1.57	−0.63	1.74	10.35	1.74	10.25	1.78	12.7
T10	1.84*	1.71	−7.07	1.95	5.84	1.99	8.22	1.86	1.08

$$y(x) = \sum_{i=1}^{l} \alpha_i K(x, x_i) + b, \tag{27}$$

where the parameters α and b are determined from equation (26) and the kernel function K (x, xi) is an arbitrary symmetric function satisfying Mercer's condition, such as K (x, y) = exp(−(x − y)2/(2σ2)).

4. Comparison of the Prediction Results Obtained from the Methods

After learning the training samples, the prediction sample set was predicted. The prediction results for the ten prediction samples are summarized in Table 3, in which the prediction results based on other methods were also listed for comparison. The maximum relative error of the BP-ANN method is up to 17.24%, and that of the LS-SVM and the RVM methods are as high as −14.7% and −14.27%, respectively. However, the RVM-PSO method has the minimum value of the maximum relative error, which is only 12.7%. To compare the prediction performances of the four methods (i.e., RVM-PSO, BP-ANN, LS-SVM, and RVM) in an intuitive manner, the predicted penetration rates and the actual values for all the test samples are drawn in Figure 5. It can be seen that the BP-ANN method provides terrible estimates for the penetration rates in samples T1, T2, T4, and T6. As for the LS-SVM method, the predictions on samples T7 and T9 significantly deviate from the measured values. When the conventional RVM method is used, there are also relatively significant differences between the predicted and actual penetration rates for samples T7 and T9. As with the RVM-PSO method, the prediction results seem close to the actual penetration rates, except for sample T9. These observations indicate that the capabilities of those four methods to predict the penetration rate are not the same, and moreover, if the test samples are sorted by the accuracies of their corresponding prediction results, the sequences are not consistent for all of those methods. Most importantly, it appears that the RVM-PSO method overall yields the best prediction. However, it is still difficult to sufficiently distinguish the capacities of those four methods to estimate the TBM penetration rate (for example, Figure 5 shows that the predictions by the LS-SVM and the conventional RVM methods are quite close for a given test sample). Hence, more reasonable and in-depth analysis is required to assess the four methods further. For this reason, some performance indices, including the mean absolute error (MAE), maximum absolute error (MXAE), mean relative error (MRE), root mean square error (RMSE), and Theil's inequality coefficient (TIC) [57], are calculated here for evaluating and comparing the prediction performances of those methods. The formulas for determining these parameters are as follows:

$$\begin{aligned}
\mathrm{MAE} &= \frac{1}{n}\sum_{i=1}^{n}\left|y_i - \widehat{y}_i\right|,\\
\mathrm{MXAE} &= \max\left|y_i - \widehat{y}_i\right|,\\
\mathrm{MRE} &= \frac{1}{n}\sum_{i=1}^{n}\frac{\left|y_i - \widehat{y}_i\right|}{y_i}\times 100\%,\\
\mathrm{RMSE} &= \sqrt{\frac{1}{n}\sum_{i=1}^{n}\left(y_i - \widehat{y}_i\right)^2},\\
\mathrm{TIC} &= \frac{\sqrt{1/n\sum_{i=1}^{n}\left(y_i - \widehat{y}_i\right)^2}}{\sqrt{\sum_{i=1}^{n} y_i^2} + \sqrt{\sum_{i=1}^{n}\widehat{y}_i^2}},
\end{aligned} \tag{28}$$

where n denotes the total number of samples; y_i and $\widehat{y}_i$ represent the measured value and the predicted value, respectively. The terms MAE, MXAE, MRE, and RMSE can reflect the prediction accuracy of the methods. The index TIC represents the level of agreement between the prediction and the real penetration rate.

The calculated values of these five parameters are delineated in Figure 6. As can be seen from Figure 6(a), there are some differences between the mean absolute errors of the predictions using the BP-ANN, LS-SVM, RVM, and RVM-PSO methods. The mean absolute error of the RVM-PSO method is only about 0.05 m/h, significantly lower than those of the other three methods. In addition, the BP-ANN method yields the highest mean absolute error, and the *MAE* value corresponding to the RVM method is lower than that generated by the LS-SVM method. Figure 6(b) shows that

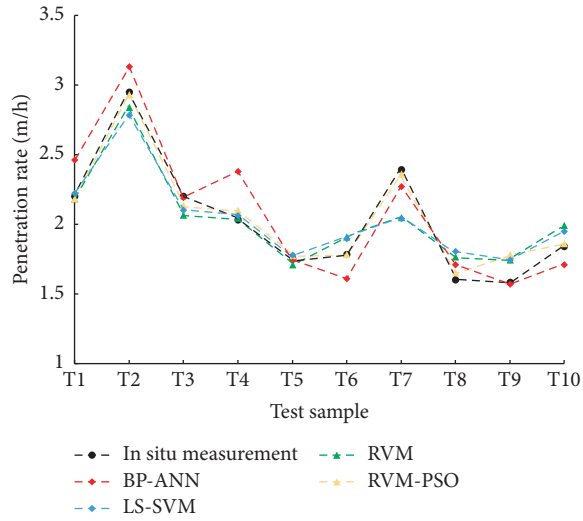

Figure 5: Comparison between the penetration rates measured in situ and those predicted using the BP-ANN, LS-SVM, RVM-PSO, and conventional RVM methods.

the RVM-PSO and LS-SVM methods give the smallest and largest values of the maximum absolute error, respectively, and the BP-ANN method produces a slightly lower MXAE than the LS-SVM method. Figure 6(c) depicts that the mean relative error (MRE) of the prediction results of the BP-ANN method is 6.53%, and that of both the LS-SVM and the RVM methods is 6.4%, while the MRE value of the RVM-PSO method is only 2.8%, even less than half of those of the former three methods. As for the remained two indices, the RVM-PSO method still generates much lower RMSE and TIC values than the other three methods, for which both the RMSE and TIC values decline from the BP-ANN to LS-SVM to RVM. Overall, it can be found from Figure 6 that the distinctions between the prediction performances of the BP-ANN, LS-SVM, and RVM methods are not very significant. More specifically, the RVM method is slightly better than the LS-SVM method, which can modify the prediction a little compared with the BP-ANN method. Most importantly, Figure 6 indicates that no matter from which index the viewpoint is, the prediction using the RVM-PSO method is always more satisfactory than that using the other three methods. Therefore, the proposed RVM-PSO method proves valid and superior for the TBM penetration rate prediction.

5. Comparison of the Effects of the Main Influencing Factors

As mentioned above, it is basically impractical to obtain the data of all the factors affecting the TBM penetration rate, and thus, it is quite interesting and useful to identify the difference in the importance of the various influencing factors for the TBM penetration rate prediction of a tunnel because this work may help researchers/engineers to ascertain or pay attention to the parameters that are significant for the penetration rate of a tunnel. In the abovementioned application example of the RVM-PSO method, five parameters are considered as the main influencing factors of the TBM penetration rate. Their importance would be evaluated and compared in this section. To this end, five new prediction models without considering each of the five influencing factors, respectively (i.e., the prediction models correspond to different combinations of just four of the five influencing factors), are established on the basis of the RVM-PSO method to predict the penetration rate. The reason for selecting the proposed RVM-PSO method is that it is already manifested to be capable of the TBM penetration rate prediction. Note that similar to the settings used in the previous section, the first fifteen groups of data listed in Table 2 are deemed as learning samples for the five new prediction models, and the remaining ten groups work as test samples. Moreover, the structures and parameters (e.g., the Gaussian kernel width and the number of iterations) of each model are consistent with those used in the previous model, in which all the five influencing factors are taken into account. Then, the five four-factor models can be applied to estimate the penetration rates in the test samples, and the importance of the five influencing factors on the penetration rate can be determined by comparing the prediction accuracies of the four-factor models with that of the previous five-factor model. By following the implementation steps described in the previous sections, the four-factor models established in this section can also make predictions of the penetration rates in the test samples. The predicted penetration rates are tabulated in Table 4.

Since the difference in the importance of the influencing factors can be reflected by the different prediction performances of the four-factor models, it is useful to compare the values of the statistic indices yielded by the models. To facilitate the comparison, the following five parameters are defined:

$$T_{1j} = \frac{\mathrm{MAE}_j}{\mathrm{MAE}_0},$$

$$T_{2j} = \frac{\mathrm{MXAE}_j}{\mathrm{MXAE}_0},$$

$$T_{3j} = \frac{\mathrm{MRE}_j}{\mathrm{MRE}_0}, \tag{29}$$

$$T_{4j} = \frac{\mathrm{RMSE}_j}{\mathrm{RMSE}_0},$$

$$T_{5j} = \frac{\mathrm{TIC}_j}{\mathrm{TIC}_0},$$

where T_{1j}, T_{2j}, ..., T_{5j} represent the ratio of the five indices (MAE, MXAE, MRE, RMSE, and TIC) yielded by the new models to those by the previous five-factor model, respectively. Values of j (=1, 2, ..., 5) correspond to the five influencing factors (α, UCS, BTS, SWP, and PSI) that are not considered in the new models in turn. For example, T_{31} represents the ratio of the *MRE* value obtained from the new model without considering α to that from the previous model. If $T_{31} > T_{32}$, this means that the mean relative error produced by the model that does not consider α, which is

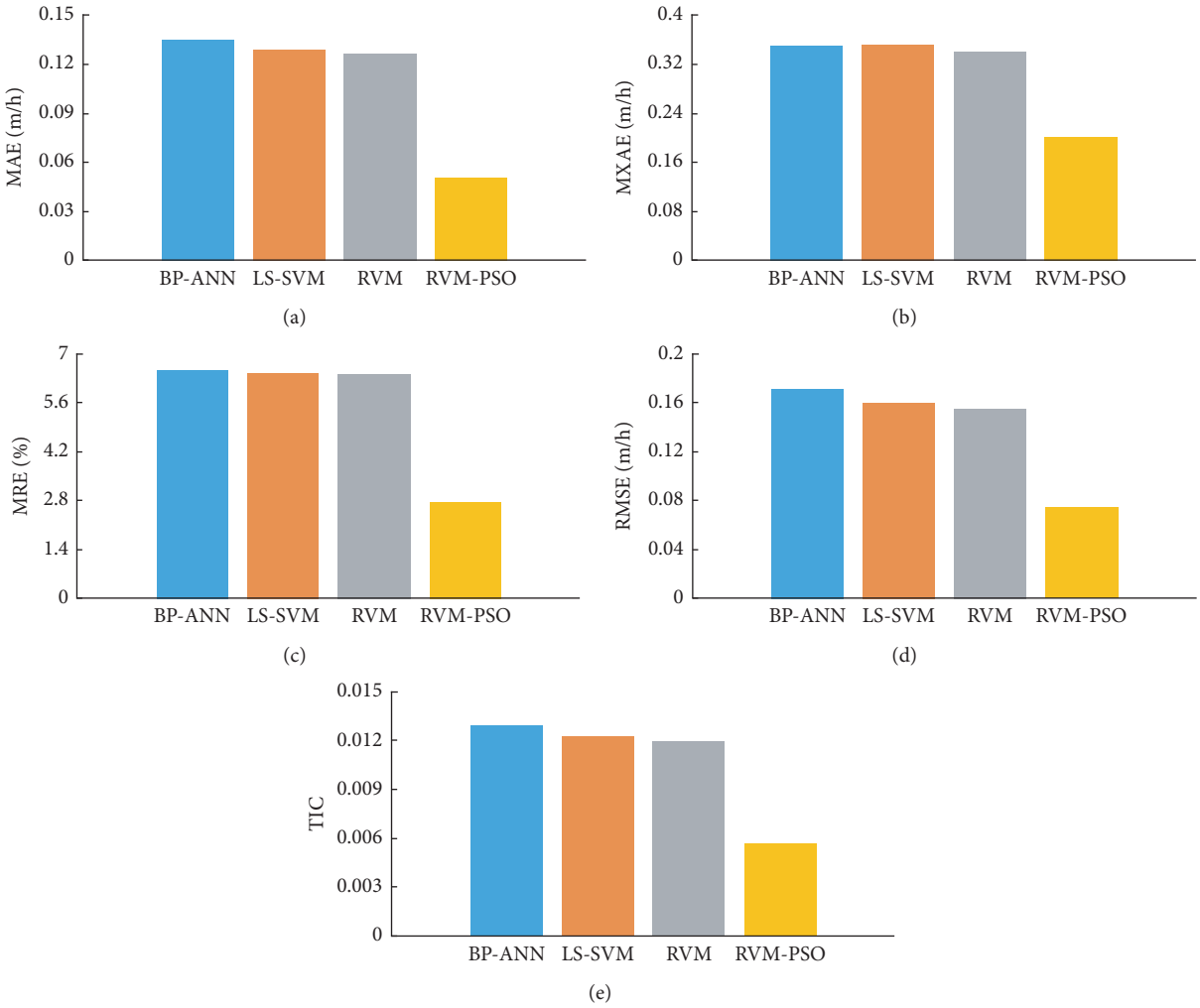

Figure 6: Comparison between the prediction performances of the four methods in terms of (a) MAE, (b) MXAE, (c) MRE, (d) RMSE, and (e) TIC.

Table 4: The predictions yielded by the five four-factor RVM-PSO models for the penetration rates (PR) in the test samples.

Sample no.	The PR (m/h) predicted using the RVM-PSO method with one missing main influencing factor				
	α	UCS	BTS	SWP	PSI
T1	2.09	2.21	2.10	2.18	2.12
T2	2.89	2.90	2.91	2.92	2.88
T3	2.05	2.13	2.07	2.10	2.06
T4	2.07	2.14	2.01	1.96	1.98
T5	1.80	1.71	1.77	1.79	1.80
T6	2.02	1.77	1.85	1.79	1.87
T7	2.04	2.27	2.15	1.97	2.30
T8	1.69	1.72	1.74	1.85	1.80
T9	1.90	1.72	1.84	2.00	1.83
T10	2.02	1.87	1.95	1.98	1.95

larger than that obtained from the one without considering UCS.

To make the Tij ($i, j = 1, 2, \ldots, 5$) values yielded by the five new models easy to compare, they are delineated in Figure 7, and the detailed Tij results are listed in Table 5. As can be seen from Figure 7 and Table 5, the values of Tij are basically larger than 1 (except for T_{22}). This means that the prediction results of the four-factor models are basically inferior to those of the previous five-factor model, indicating that each of the five main influencing factors indeed affects the prediction results and the five main influencing factors selected in the previous sections are reasonable. Moreover, for a given value of i, the values of Tij are usually not the same when j varies, suggesting that the importance of the five influencing factors is different for the TBM penetration rate prediction of the Queens Water Tunnel #3. It is observed that T_{i1} and T_{i4} are always larger than T_{i2}, T_{i3}, and T_{i5}, and the difference between T_{i1} and T_{i4} is not very conspicuous for any value of i; therefore, the angle between the longitudinal tunnel axis and the plane of weakness (i.e., α) and the spacing between the weakness planes (SWP) have significant effects.

Moreover, for a fixed value of i, T_{i3} and T_{i5} are basically equal; hence, the importance of the Brazilian tensile strength

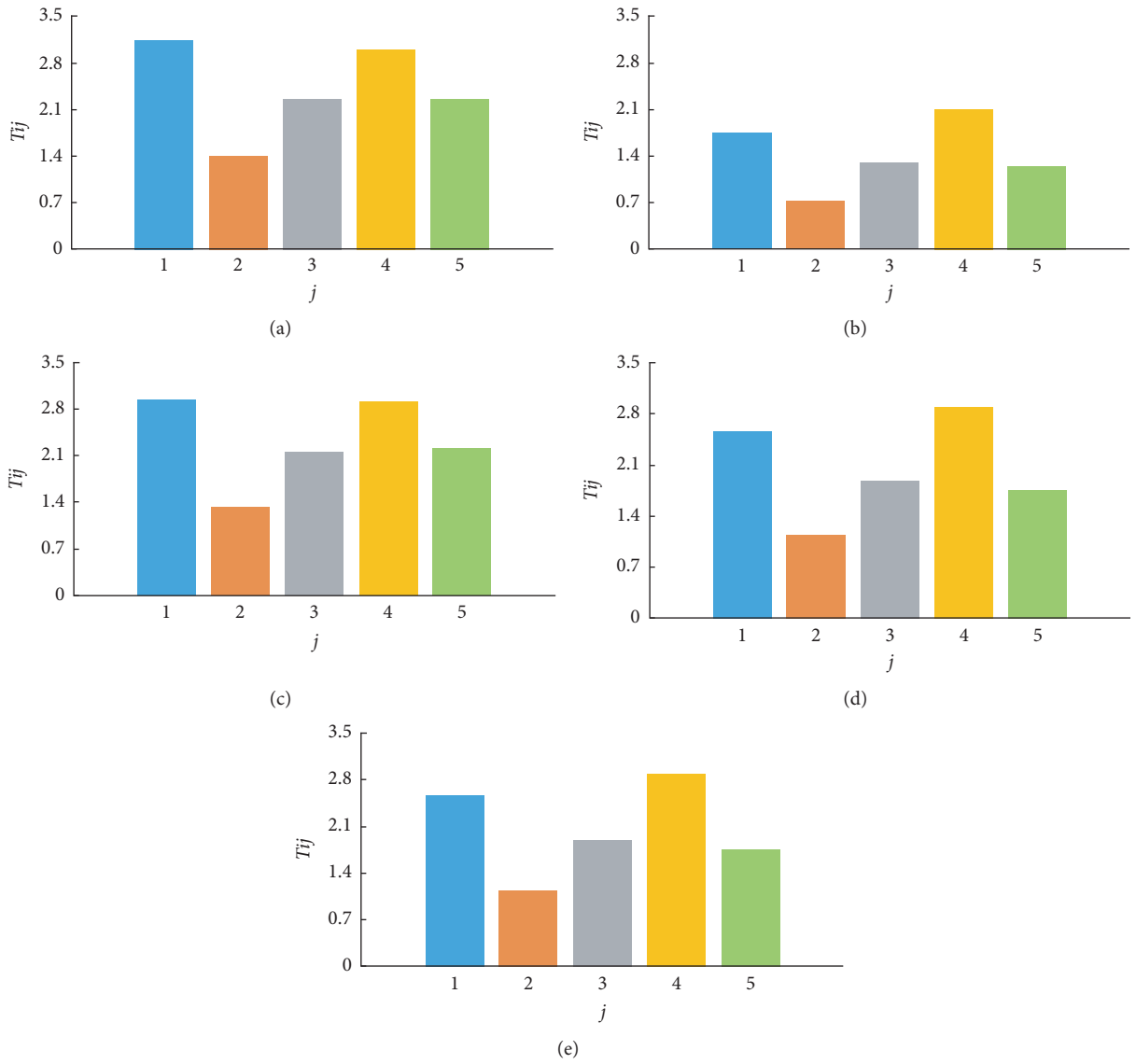

Figure 7: The T_{ij} values induced by the five four-factor RVM-PSO models for the cases of (a) $i = 1$, (b) $i = 2$, (c) $i = 3$, (d) $i = 4$, and (e) $i = 5$.

Table 5: The T_{ij} values induced by the five four-factor RVM-PSO models for the predictions of the penetration rates in the test samples.

i	T_{ij}				
	$j = 1$	$j = 2$	$j = 3$	$j = 4$	$j = 5$
1	2.95	1.34	2.15	2.92	2.22
2	2.56	1.14	1.89	2.89	1.76
3	3.14	1.41	2.27	3	2.27
4	1.74	0.72	1.31	2.11	1.26
5	2.57	1.15	1.90	2.89	1.76

(BTS) and that of the peak slope index are nearly the same for this tunnel practice. In addition, Figure 7 clearly shows that the model without considering the UCS has the closest prediction performance to the previous five-factor model, and the mean relative error yielded by the former is only 3.71%. These observations imply that the UCS has a smaller influence on the TBM penetration rate prediction of the Queens Water Tunnel #3 than the other four factors, while α and SWP are quite important for the prediction. Therefore, in the penetration rate prediction of that tunnel, data of UCS might be able to leave out for the purpose of reducing workload, but the acquisition of α and SWP should be paid more attention.

In practical engineering, it is quite difficult to acquire the detailed data of all the factors affecting the TBM penetration rate, and even the data of some important factors might not be collected. Hence, it is meaningful to assess the predictive ability of the proposed RVM-PSO model under the working condition that not the data of all the main influencing factors are available. For comparison, both the RVM-PSO and the conventional RVM methods are employed to estimate the penetration rates in the test samples listed in Table 2, under the assumption that the values of α or SWP are not known. In other words, both the RVM-PSO and RVM models

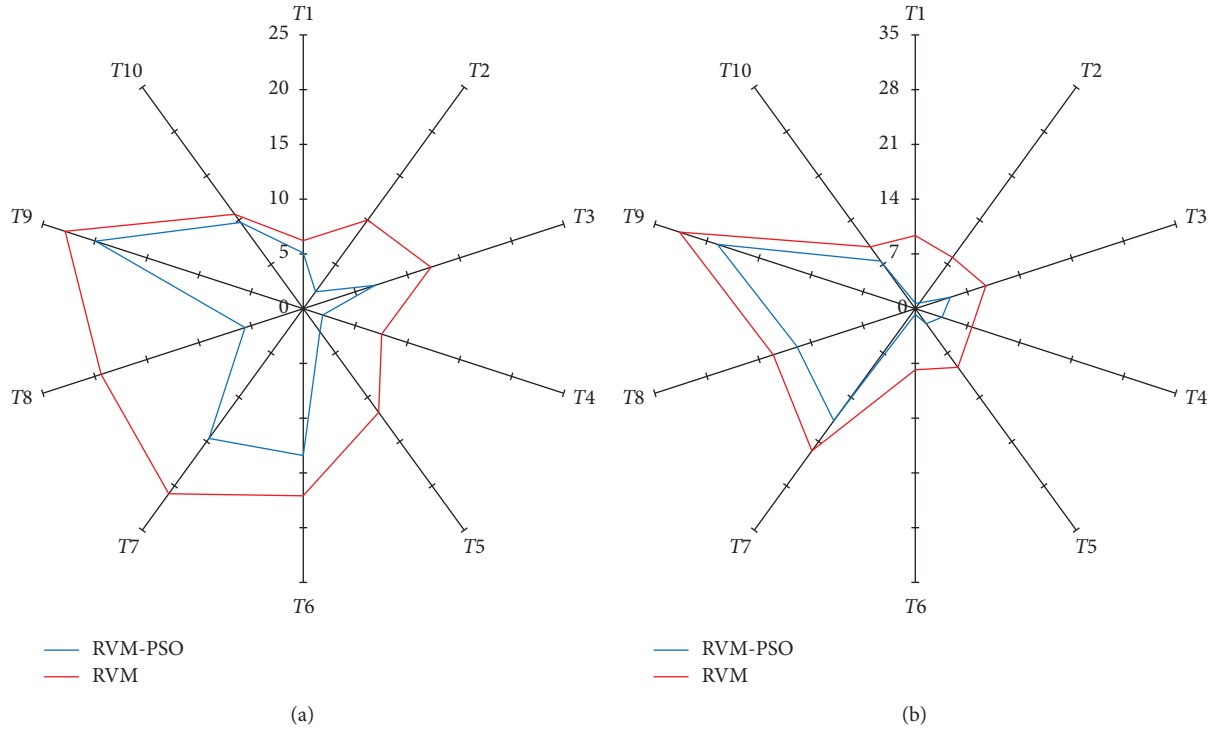

Figure 8: The relative errors (%) of the penetration rates predicted using the RVM-PSO and the conventional RVM methods without considering (a) α and (b) SWP.

compared here belong to the four-parameter model without considering α or SWP. The reason for selecting the RVM method (instead of the BP-ANN and LS-SVM methods) to be compared with the RVM-PSO method here is that the RVM is already proved to be more accurate than the BP-ANN and LS-SVM for TBM penetration rate prediction, as shown in the previous section. Figure 8 presents the relative errors of the penetration rates predicted by the RVM-PSO and the conventional RVM methods when α or SWP is not taken into account in the predictions. It can be found that the RVM-PSO method always generates smaller errors in the prediction than the RVM for each of the test samples, no matter for the absence of α or SWP. Thus, the RVM-PSO method is superior to the RVM method. Moreover, even when one of the two most important influencing factors identified for the TBM penetration rate prediction of the Queens Water Tunnel #3 is not considered, the mean relative error yielded by the RVM-PSO method is about 8%, less than 10%. Therefore, the RVM-PSO method is useful to estimate the TBM penetration rate in rock tunnels, and it has a relatively good tolerance for missing or lacking the data of a few influencing factors.

6. Conclusions

Accurate prediction of the TBM penetration rate is of great significance to tunnel constructions, for purposes of optimizing design schemes, saving economic costs, and evaluating the feasibility of engineering constructions. Thus, a useful intelligent method, RVM-PSO, is developed to estimate the penetration rate of the TBM. To check the validity of the developed method, it was applied to the prediction of the TBM penetration rate in the Queens Water Tunnel #3. Then, the prediction performance of the RVM-PSO method was compared with that of the BP-ANN, LS-SVM, and conventional RVM methods. The main conclusions are drawn as follows:

(1) The penetration rate of the TBM is affected by various factors, and there are complex nonlinear relationships between the penetration rate and its influencing factors. The RVM-PSO method developed in this study can effectively establish a nonlinear correlation between the penetration rate and its main influencing factors and can achieve a relatively good prediction of the TBM penetration rate.

(2) The RVM-PSO method proves able to provide much better prediction than the BP-ANN, LS-SVM, and RVM. In addition, the BP-ANN and the LS-SVM methods have close prediction performances, and they are inferior to the RVM. Moreover, even if there is a lack of data on an important factor affecting the penetration rate, the prediction yielded by the RVM-PSO method is still more accurate than that using the RVM.

(3) The RVM-PSO method is useful in identifying the difference in the importance of the various factors affecting the TBM penetration rate prediction. It can help researchers/engineers to pay attention to the parameters that are significant for the penetration rate prediction and to leave out the data acquisition

of the nonsignificant influencing factors in order to reduce workload.

Data Availability

The data used to support the findings of this study are available from the corresponding author upon request.

Conflicts of Interest

The authors declare no conflicts of interest.

Acknowledgments

The authors are grateful for the financial support from the National Natural Science Foundation of China (grant nos. 51409051 and 51869003), the Systematic Project of Guangxi Key Laboratory of Disaster Prevention and Structural Safety (grant no. 2019ZDK023), the Guangxi Key Laboratory of New Energy and Building Energy Saving (grant no. 19-J-21-22), the High Level Innovation Team and Outstanding Scholar Program of Universities in Guangxi Province (2020), and the Guangxi Natural Science Foundation (grant no. 2020GXNSFAA159125).

References

[1] A. Li, Y. Liu, F. Dai, K. Liu, and M. Wei, "Continuum analysis of the structurally controlled displacements for large-scale underground caverns in bedded rock masses," *Tunnelling and Underground Space Technology*, vol. 97, Article ID 103288, 2020.

[2] N. Xu, F. Dai, B. Li, Y. Zhu, T. Zhao, and D. Yang, "Comprehensive evaluation of excavation-damaged zones in the deep underground caverns of the Houziyan hydropower station, Southwest China," *Bulletin of Engineering Geology and the Environment*, vol. 76, no. 1, pp. 275–293, 2017.

[3] F. Dai, B. Li, N. Xu, Y. Fan, and C. Zhang, "Deformation forecasting and stability analysis of large-scale underground powerhouse caverns from microseismic monitoring," *International Journal of Rock Mechanics and Mining Sciences*, vol. 86, pp. 269–281, 2016.

[4] L. H. Hu, Y. C. Li, X. Liang, C. A. Tang, and L. B. Yan, "Rock damage and energy balance of strainbursts induced by low frequency seismic disturbance at high static stress," *Rock Mechanics and Rock Engineering*, 2020.

[5] L. Hu, G. Su, X. Liang, Y. Li, and L. Yan, "A distinct element based two-stage-structural model for investigation of the development process and failure mechanism of strainburst," *Computers and Geotechnics*, vol. 118, Article ID 103333, 2020.

[6] Y. Liu, F. Dai, L. Dong, N. Xu, and P. Feng, "Experimental investigation on the fatigue mechanical properties of intermittently jointed rock models under cyclic uniaxial compression with different loading parameters," *Rock Mechanics and Rock Engineering*, vol. 51, no. 1, pp. 47–68, 2018.

[7] M.-D. Wei, F. Dai, N.-W. Xu, T. Zhao, and Y. Liu, "An experimental and theoretical assessment of semi-circular bend specimens with chevron and straight-through notches for mode I fracture toughness testing of rocks," *International Journal of Rock Mechanics and Mining Sciences*, vol. 99, pp. 28–38, 2017.

[8] M.-D. Wei, F. Dai, N.-W. Xu, Y. Liu, and T. Zhao, "A novel chevron notched short rod bend method for measuring the mode I fracture toughness of rocks," *Engineering Fracture Mechanics*, vol. 190, pp. 1–15, 2018.

[9] M.-D. Wei, F. Dai, J.-W. Zhou, Y. Liu, and J. Luo, "A further improved maximum tangential stress criterion for assessing mode I fracture of rocks considering non-singular stress terms of the Williams expansion," *Rock Mechanics and Rock Engineering*, vol. 51, no. 11, pp. 3471–3488, 2018.

[10] P. Feng, F. Dai, Y. Liu, N. W. Xu, and P. X. Fan, "Effects of coupled static and dynamic strain rates on the mechanical behaviors of rock-like specimens containing preexisting fissures under uniaxial compression," *Canadian Geotechnical Journal*, vol. 55, no. 5, pp. 640–652, 2017.

[11] P. Feng, M. Wei, F. Dai, R. Tang, H. Qiu, and J. Gong, "DEM investigation on the mechanical behaviors of flawed specimens subjected to coupled static-dynamic loads," *Soil Dynamics and Earthquake Engineering*, vol. 135, pp. 106–220, 2020.

[12] N. Barton, "TBM performance estimation in rock using QTBM," *Tunnels and Tunnelling International*, vol. 31, no. 9, pp. 30–34, 1999.

[13] S. Yagiz, "New equations for predicting the field penetration index of tunnel boring machines in fractured rock mass," *Arabian Journal of Geosciences*, vol. 10, no. 2, pp. 1–13, 2017.

[14] L. J. Yin, Q. M. Gong, and J. Zhao, "Study on rock mass boreability by TBM penetration test under different in situ stress conditions," *Tunnelling and Underground Space Technology*, vol. 43, pp. 413–425, 2014.

[15] J. Rostami, "Development of a force estimation model for rock fragmentation with disc cutters through theoretical modeling and physical measurement of crushed zone pressure," Ph. D. Thesis, Colorado School of Mines, Golden, CO, USA, 1997.

[16] A. Bruland, "Hard rock tunnel boring," Ph. D. Thesis, Norwegian University of Science and Technology, Trondheim, Norway, 1998.

[17] A. G. Benardos and D. C. Kaliampakos, "Modelling TBM performance with artificial neural networks," *Tunnelling and Underground Space Technology*, vol. 19, no. 6, pp. 597–605, 2004.

[18] J. Gholamnejad and N. Tayarani, "Application of artificial neural networks to the prediction of tunnel boring machine penetration rate," *Mining Science and Technology*, vol. 20, no. 5, pp. 727–733, 2010.

[19] S. Mahdevari, K. Shahriar, S. Yagiz, and M. Akbarpour Shirazi, "A support vector regression model for predicting tunnel boring machine penetration rates," *International Journal of Rock Mechanics and Mining Sciences*, vol. 72, pp. 214–229, 2014.

[20] L. Gao and X.-b. Li, "Utilizing partial least square and support vector machine for TBM penetration rate prediction in hard rock conditions," *Journal of Central South University*, vol. 22, no. 1, pp. 290–295, 2015.

[21] M. Koopialipoor, S. S. Nikouei, A. Marto, A. Fahimifar, D. Jahed Armaghani, and E. T. Mohamad, "Predicting tunnel boring machine performance through a new model based on the group method of data handling," *Bulletin of Engineering Geology and the Environment*, vol. 78, no. 5, pp. 3799–3813, 2019.

[22] A. Salimi, J. Rostami, C. Moormann, and A. Delisio, "Application of non-linear regression analysis and artificial intelligence algorithms for performance prediction of hard rock TBMs," *Tunnelling and Underground Space Technology*, vol. 58, pp. 236–246, 2016.

[23] S. Yagiz, C. Gokceoglu, E. Sezer, and S. Iplikci, "Application of two non-linear prediction tools to the estimation of tunnel

boring machine performance," *Engineering Applications of Artificial Intelligence*, vol. 22, no. 4–5, pp. 808–814, 2009.

[24] R. Mikaeil, M. Z. Naghadehi, and F. Sereshki, "Multifactorial fuzzy approach to the penetrability classification of TBM in hard rock conditions," *Tunnelling and Underground Space Technology*, vol. 24, no. 5, pp. 500–505, 2009.

[25] S. Wen, T. X. Zhao, and S. Q. Yang, "Prediction on penetration rate of TBM based on Monte Carlo-BP neural network," *Rock Soil Mech*, vol. 30, no. 10, pp. 3127–3132, 2009.

[26] S. Yagiz and H. Karahan, "Prediction of hard rock TBM penetration rate using particle swarm optimization," *International Journal of Rock Mechanics and Mining Sciences*, vol. 48, no. 3, pp. 427–433, 2011.

[27] E. Ghasemi, S. Yagiz, and M. Ataei, "Predicting penetration rate of hard rock tunnel boring machine using fuzzy logic," *Bulletin of Engineering Geology and the Environment*, vol. 73, no. 1, pp. 23–35, 2014.

[28] S. Yagiz and H. Karahan, "Application of various optimization techniques and comparison of their performances for predicting TBM penetration rate in rock mass," *International Journal of Rock Mechanics and Mining Sciences*, vol. 80, pp. 308–315, 2015.

[29] R. Mikaeil, M. Zare Naghadehi, and S. Ghadernejad, "An extended multifactorial fuzzy prediction of hard rock TBM penetrability," *Geotechnical and Geological Engineering*, vol. 36, no. 3, pp. 1779–1804, 2018.

[30] M. Z. Naghadehi, M. Samaei, M. Ranjbarnia, and V. Nourani, "State-of-the-art predictive modeling of TBM performance in changing geological conditions through gene expression programming," *Measurement*, vol. 126, pp. 46–57, 2018.

[31] M. Samaei, M. Ranjbarnia, V. Nourani, and M. Zare Naghadehi, "Performance prediction of tunnel boring machine through developing high accuracy equations: a case study in adverse geological condition," *Measurement*, vol. 152, Article ID 107244, 2020.

[32] M. Z. Naghadehi, M. Samaei, and M. Ranjbarnia, "Superior modeling of hard rock TBM performance using novel predictive analytics methodologies," in *Proceedings of the 3rd International Conference on Applied Reseaches in Structural Engineering and Constrution Management*, Sharif University of Technology, Tehran, Iran, pp. 1–11, June 2019.

[33] D. Tien Bui, V.-H. Nhu, and N.-D. Hoang, "Prediction of soil compression coefficient for urban housing project using novel integration machine learning approach of swarm intelligence and multi-layer perceptron neural network," *Advanced Engineering Informatics*, vol. 38, pp. 593–604, 2018.

[34] D. J. Armaghani, M. Hajihassani, E. T. Mohamad, A. Marto, and S. A. Noorani, "Blasting-induced flyrock and ground vibration prediction through an expert artificial neural network based on particle swarm optimization," *Arabian Journal of Geosciences*, vol. 7, no. 12, pp. 5383–5396, 2014.

[35] H.-B. Zhao and S. Yin, "Geomechanical parameters identification by particle swarm optimization and support vector machine," *Applied Mathematical Modelling*, vol. 33, no. 10, pp. 3997–4012, 2009.

[36] A. Nazari and S. Riahi, "Prediction split tensile strength and water permeability of high strength concrete containing TiO_2 nanoparticles by artificial neural network and genetic programming," *Composites Part B: Engineering*, vol. 42, no. 3, pp. 473–488, 2011.

[37] N. D. Hoang and D. Tien Bui, "A novel relevance vector machine classifier with cuckoo search optimization for spatial prediction of landslides," *Journal of Computing in Civil Engineering*, vol. 30, no. 5, Article ID 04016001, 2016.

[38] M. Clerc and J. Kennedy, "The particle swarm-explosion, stability, and convergence in a multidimensional complex space," *IEEE Transactions on Evolutionary Computation*, vol. 6, no. 1, pp. 58–73, 2002.

[39] M. E. Tipping, "Sparse bayesian learning and the relevance vector machine," *Journal of Machine Learning Research*, vol. 1, pp. 211–244, 2001.

[40] R. C. Eberhart and J. Kennedy, "A new optimizer using particle swarm theory," in *Proceedings of the Sixth International Symposium on Micro Machine and Human Science*, pp. 39–43, Nagoya, Japan, October 1995.

[41] D. Tien Bui, B. Pradhan, H. Nampak, Q.-T. Bui, Q.-A. Tran, and Q.-P. Nguyen, "Hybrid artificial intelligence approach based on neural fuzzy inference model and metaheuristic optimization for flood susceptibilitgy modeling in a high-frequency tropical cyclone area using GIS," *Journal of Hydrology*, vol. 540, pp. 317–330, 2016.

[42] X.-T. Feng, B.-R. Chen, C. Yang, H. Zhou, and X. Ding, "Identification of visco-elastic models for rocks using genetic programming coupled with the modified particle swarm optimization algorithm," *International Journal of Rock Mechanics and Mining Sciences*, vol. 43, no. 5, pp. 789–801, 2006.

[43] R. Ojha and M. Das, "An adaptive approach for modifying inertia weight using particle swarm optimisation," *International Journal of Computational Science*, vol. 9, pp. 105–111, 2012.

[44] S. Yagiz, "Utilizing rock mass properties for predicting TBM performance in hard rock condition," *Tunnelling and Underground Space Technology*, vol. 23, no. 3, pp. 326–339, 2008.

[45] X. Fan, P. H. S. W. Kulatilake, and X. Chen, "Mechanical behavior of rock-like jointed blocks with multi-non-persistent joints under uniaxial loading: a particle mechanics approach," *Engineering Geology*, vol. 190, no. 5, pp. 17–32, 2015.

[46] X. Fan, K. Li, H. Lai, Y. Xie, R. Cao, and J. Zheng, "Internal stress distribution and cracking around flaws and openings of rock block under uniaxial compression: a particle mechanics approach," *Computers and Geotechnics*, vol. 102, no. 10, pp. 28–38, 2018.

[47] W. Wu, J. C. Li, and J. Zhao, "Loading rate dependency of dynamic responses of rock joints at low loading rate," *Rock Mechanics and Rock Engineering*, vol. 45, no. 3, pp. 421–426, 2012.

[48] W. Wu and J. Zhao, "Effect of water content on P-wave attenuation across a rock fracture filled with granular materials," *Rock Mechanics and Rock Engineering*, vol. 48, no. 2, pp. 867–871, 2015.

[49] H.-b. Du, F. Dai, Y. Xu, Z. Yan, and M.-d. Wei, "Mechanical responses and failure mechanism of hydrostatically pressurized rocks under combined compression-shear impacting," *International Journal of Mechanical Sciences*, vol. 165, p. 105219, 2020.

[50] W. Wu and J. Zhao, "A Dynamic-induced direct-shear model for dynamic triggering of frictional slip on simulated granular gouges," *Experimental Mechanics*, vol. 54, no. 4, pp. 605–613, 2014.

[51] K. Duan, Y. Li, L. Wang, G. Zhao, and W. Wu, "Dynamic responses and failure modes of stratified sedimentary rocks," *International Journal of Rock Mechanics and Mining Sciences*, vol. 122, p. 104060, 2019.

[52] W. Wu, H. Li, and J. Zhao, "Dynamic responses of non-welded and welded rock fractures and implications for P-wave attenuation in a rock mass," *International Journal of Rock Mechanics and Mining Sciences*, vol. 77, pp. 174–181, 2015.

[53] Y. Xu and F. Dai, "Dynamic response and failure mechanism of brittle rocks under combined compression-shear loading experiments," *Rock Mechanics and Rock Engineering*, vol. 51, no. 3, pp. 747–764, 2018.

[54] M. D. Wei, F. Dai, N. W. Xu, T. Zhao, and K. W. Xia, "Experimental and numerical study on the fracture process zone and fracture toughness determination for ISRM-suggested semi-circular bend rock specimen," *Engineering Fracture Mechanics*, vol. 154, pp. 43–56, 2016.

[55] J. L. McClelland and D. E. Rumelhart, *Parallel Distributed Processing: Explorations in the Microstructure of Cognition. 2, Psychological and Biological Models*, MIT Press, Cambridge, MA, USA, 1986.

[56] J. A. K. Suykens, T. Van Gestel, J. De Brabanter, B. De Moor, and J. Vandewalle, *Least Squares Support Vector Machines*, World Scientific Publishing Co. Pvt. Ltd., KU Leuven, Belgium, 2002.

[57] D. J. Murray-Smith, "Methods for the external validation of continuous system simulation models," *Mathematical and Computer Modelling of Dynamical Systems*, vol. 4, no. 1, pp. 5–31, 1998.